Molecular architecture and platelet-activating properties of small immune complexes assembled on heparin and platelet factor 4

Check for updates

Yang Yang[1], Yi Du[1], Daniil Ivanov[1], Chendi Niu[1], Rumi Clare[2], James W. Smith[2], Ishac Nazy[2] & Igor A. Kaltashov [1] ✉

Heparin-induced thrombocytopenia (HIT) is an adverse reaction to heparin leading to a reduction in circulating platelets with an increased risk of thrombosis. It is precipitated by polymerized immune complexes consisting of pathogenic antibodies that recognize a small chemokine platelet factor 4 (PF4) bound to heparin. Characterization of these immune complexes is extremely challenging due to the enormous structural heterogeneity of such macromolecular assemblies and their constituents. Native mass spectrometry demonstrates that up to three PF4 tetramers can be assembled on a heparin chain, consistent with the molecular modeling studies showing facile polyanion wrapping along the polycationic belt on the PF4 surface. Although these assemblies can accommodate a maximum of only two antibodies, the resulting immune complexes are capable of platelet activation despite their modest size. Taken together, these studies provide further insight into molecular mechanisms of HIT and other immune disorders where anti-PF4 antibodies play a central role.

Platelet factor 4 (PF4) is a chemokine that is secreted from activated platelets[1] and involved in a variety of physiological processes, ranging from coagulation and tissue repair to innate immune response[2]. It has gained particular notoriety due to its role in triggering a range of (auto)immune hematologic pathologies, the first of which—heparin-induced thrombocytopenia (HIT)—was initially reported sixty-five years ago[3]. More recently it was implicated in thrombotic complications accompanying rare but potentially fatal side effects of adenoviral-vectored COVID-19 vaccines, presently known as vaccine-induced immune thrombotic thrombocytopenia (VITT)[4]. A common feature of these disorders is the formation of large immune complexes, in which multiple PF4 tetramers polymerize anti-PF4 antibodies. This leads to clustering of FcγRIIa receptors on the platelet surface, thereby initiating cross-phosphorylation of the Immunoreceptor Tyrosine-based Activation Motifs (ITAMs) within their cytosolic parts[5], which is the first step in the platelet activation cascade[6]. While the sequence of events leading to the onset of HIT has been known for some time, the actual occurrence of this pathology among heparin patients (including those that produce anti-PF4 antibodies) appears to be random and impossible to predict (as is the occurrence of VITT among vaccinated individuals).

The structure of the PF4-based immune complexes must be one of the major determinants of the occurrence of HIT and the progression of this pathology, but its detailed characterization at the molecular level is extremely challenging due to both macro-heterogeneity of such assemblies and micro-heterogeneity of their constituents. The macro-heterogeneity refers to the broad distribution of sizes exhibited by both immune complexes and their precursors—PF4/heparin assemblies[7]. The latter are usually classified based on their elution behavior in size exclusion chromatography (SEC) as either small or ultra-large complexes (SCs and ULCs, respectively). SCs are considered precursors to ULCs, and elucidation of the architecture of the SCs (involving only a single heparin chain) is important not only for understanding their specific role in HIT pathogenesis, but also for building a molecular model of ULCs. Both SCs and ULCs exhibit a range of sizes and stoichiometries, although there is evidence suggesting that equimolar PF4:heparin stoichiometry is optimal vis-à-vis the formation of ULCs, which are more pathogenic[8].

The micro-heterogeneity refers to the structural diversity within the constituents of both SCs and ULCs, which is mostly due to the variation of heparin chain length and its sulfation and acetylation patterns[9,10], although

[1]Department of Chemistry, University of Massachusetts-Amherst, Amherst, MA, USA. [2]Department of Biochemistry and Biomedical Sciences, McMaster University, Hamilton, Canada. ✉e-mail: kaltasho@umass.edu

some variability within the circulating PF4 has also been noted[11]. Because of the extensive heterogeneity exhibited by the PF4/heparin complexes, their initial characterization relied on relatively low-resolution methods of structural analysis, such as SEC[8,12,13].

Meaningful utilization of high-resolution methods capable of providing detailed structural information is also possible, but requires both the size and the heterogeneity of the relevant macromolecular assemblies to be reduced dramatically, *e.g.* to enable their crystallization and recording of interpretable diffraction patterns. This was recently accomplished by Cai et al.[14], who not only solved the crystal structure of recombinant PF4 complexed to a small (pentasaccharide) synthetic heparinoid, fondaparinux, but were also able to obtain an atomic-level structure of the fondaparinux-bound PF4 associated with a Fab segment of a monoclonal anti-PF4/heparin antibody (KKO)[15] that mimics the behavior of human HIT antibodies. One important feature of the PF4/fondaparinux complexes revealed in that study is the allosteric change within the PF4 tetramers induced by the short polyanion binding, which exposes a neo-epitope on the protein surface and enables its recognition by KKO (and, by extension, pathogenic wild-type HIT antibodies)[14]. However, because of the small size of the complex and the homogeneity of its constituents (unlike heparin, fondaparinux is chemically defined, and its length is only 1/10 of the average heparin chain), the structure of the pathogenic PF4/heparin complexes could not be determined directly, but instead was inferred by extrapolating the features of the relatively small and homogeneous PF4/fondaparinux assemblies to a larger scale[14]. One particularly intriguing conclusion was that PF4 tetramer binding to the heparin chain "*imparts a local linearized structure*" within the latter, thereby enhancing binding of the second PF4 molecule[14]. It was suggested that progression of this process should lead to formation of a large antigenic complex, in which PF4 tetramers cluster around a semi-rigid heparin chain[14]. This scenario differs from the earlier models of PF4/heparin complexes, in which the anionic polysaccharide is wrapped around the tetramer along its equatorial belt where the basic amino acids are localized[16]. The conformational bias towards the linearized chains upon heparin/PF4 association envisioned by Cai and co-workers[14] has important ramifications, as it would allow high-density protein tethering to a single polyanion chain, which would enable effective platelet activation by immune complexes assembled on a single heparin chain compared to the classical models[16] (which imply a much lower number of PF4 tetramers bound to a single heparin chain—and, therefore, a lower number of anti-PF4/heparin antibodies that can associate with such complexes). However, characterization of the molecular architecture of the clinically relevant PF4/heparin assemblies and HIT-related immune complexes based upon them remained outside of the reach of experimental biophysics.

In the past two decades mass spectrometry (MS) proved to be a powerful tool for characterization of non-covalent biopolymer assemblies; however, its utility in the field of protein-glycosaminoglycan (GAG) interactions remains confined to systems with limited size and modest structural heterogeneity[17–19]. The progress made in the field of MS-based analysis of highly heterogeneous systems, and particularly incorporation of ion chemistry in the MS workflow[20] (such as the limited charge reduction technique[21,22]) resulted in a dramatic expansion of the scope of macromolecules and their assemblies for which meaningful information can be obtained. In this work we employ native MS supplemented with limited charge reduction to study association of PF4 with intact unfractionated heparin (UFH), revealing a range of binding stoichiometries within SCs. Although the largest assembly within this set corresponds to only three PF4 tetramers accommodated by a single heparin chain (consistent with the classical model of PF4/heparin interaction[16] and confirmed by molecular modeling), the corresponding immune complexes may incorporate up to two antibody molecules, as revealed by native MS. Importantly, the results of platelet activation assays show that such immune complexes are capable of triggering platelet activation, and are a surrogate marker for the HIT disease. This poses an intriguing question of whether the minimal size of the FcγRIIa clusters on the platelet surface required for its activation is indeed two, or the initial immune complex incorporating only two antibody molecules serves

only as a seed for a large FcγRIIa cluster formation on the platelet surface, a process facilitated by the dimensionality reduction (from 3D in circulation to 2D on the cell surface). The picture of the SC molecular organization emerging from this work also provides important insights vis-à-vis architecture of ULCs, the MDa-size PF4/heparin assemblies that are commonly considered to be the critical element in triggering HIT.

Results

PF4/heparin association: polyanion chain length as the major determinant of the SC architecture and evidence supporting the "wrap-around" interaction model

Close approximation of at least two PF4 tetramers is key to formation of an immune complex capable of activating platelets[13], although it remains unclear if there is a minimal heparin chain length that enables such protein clustering. Previously we have shown that short heparin fragments (at least up to a decasaccharide level, dp10) are not sufficient for PF4 bridging (instead, multiple heparinoids associate with a single PF4 tetramer)[23]. Similar behavior is exhibited by significantly longer chains, such as dp20 (the length that corresponds to an average size of the low-molecular weight heparin products, LMWH[24]), as can be seen in Fig. 1A. Incubation of dp20 with PF4 at an approximately equimolar ratio gives rise to an abundant ionic signal corresponding to a PF4·(dp20)$_2$ complex, although the 1:1 protein/heparinoid complexes are also observed (Fig. 1A, top). Mass measurements of the most abundant species in both distributions indicates that average mass of dp20 species incorporated in the PF4·(dp20)$_2$ complex is slightly higher compared to that within the PF4·dp20 complex (the average mass of the protein-bound dp20 increases by *ca.* 170 Da, which corresponds to two additional sulfate groups), indicating the preference for more extensively sulfated species within the former. Higher concentration of dp20 in the protein/heparinoid mixture results in a near-complete elimination of the PF4·dp20 complexes, and a signal shift for the PF4·(dp20)$_2$ species towards higher *m/z* values (Fig. 1A, bottom). This mass increase (0.25–0.3 kDa) is indicative of the increased extent of sulfation of the protein-bound heparinoid chains (three to four "extra" sulfate groups per each heparinoid chain), consistent with the notion of the high charge density being the most important factor vis-à-vis heparin binding preferences to polycationic proteins[25]. We also note the absence of the putative complexes formed by bridging of two (or more) PF4 tetramers by a single dp20 chain. The surprisingly limited range of stoichiometries exhibited by the PF4/dp20 complexes is in contrast with the models of the small complexes formed by PF4 and a slightly shorter heparin oligomer (dp18) that was recently described by Shi et al.[26], which envisioned not only the possibility of bridging two PF4 tetramers by a single heparinoid chain, but also accommodation of up to five dp18 chains by a single PF4 tetramer. Despite being inconsistent with the Shi model, our experimental results are corroborated by the molecular modeling work carried out in our laboratory, which provides a clear indication that the positive charge basin around the PF4 tetramer can readily accommodate only up to two dp20 chains (Fig. 1B). The polyanioinic chain persistence length (heparin's Kuhn segment length is 9 ± 2 nm[27]) is small compared to the protein dimensions (the diameter of PF4 tetramer is 52 ± 3 nm), which allows the heparin oligomer to maximize the electrostatic interactions by circumscribing the PF4 surface. The dp20 chain length is nearly one-half of the protein circumference, which allows a single PF4 tetramer to accommodate a maximum of two such polyanions (Fig. 1B). The continuity of the positive charge belt on the PF4 surface and the high (and nearly uniform) negative charge density across the heparin oligomer chain (2.7 sulfate groups and one carboxylic group per single disaccharide[28]) are the two major determinants of the wrap-around mode of interaction (as depicted in Fig. 1B) having the lowest free energy, as it is this configuration of the complex that maximizes the attractive electrostatic interactions in this system.

Binding of multiple (up to three) PF4 tetramers to a single polyanion chain becomes evident only when unfractionated heparin (UFH) is used as an assembly scaffold. Consistent with an earlier study by Rauova et al.[8], the SEC chromatogram of a PF4/UFH mixture (Fig. 2A) displays two distinct

peaks representing ULCs (elution window 6–7 min) and SCs (9.5–12 min). An estimate of the molecular weights of the species constituting SCs (based on their elution time in the chromatogram) yields a 30–130 kDa MW range (see Figure S1 in Supplementary Material for more detail). Fractionation of this peak enables isolation of PF4/heparin assemblies of varying dimensions (Fig. 2A), although the stoichiometries of the putative $(PF4)_n \cdot (heparin)_m$ complexes comprising each subfraction cannot be confidently assigned based on the elution time alone; instead, this task was accomplished by MS analysis of each collected sub-fraction.

Native MS analysis of the latest-eluting SCs subfraction (the collection window 11.0–11.5 min) yields a mass spectrum that contains an abundant ionic signal within a relatively narrow m/z range (3500–4500), but does not display any resolved charge states (Fig. 2B, top trace). The three other subfractions give rise to even more convoluted ionic signals, which gradually shift towards higher m/z values. Overall, three discernable features are observed in the mass spectra of the four SCs subfractions (confined to m/z regions 3500–4500; 4500–6000 and 6000–8000), indicating the presence of three distinct species in solution that differ from each other in size. The abundance of the lowest-m/z species gradually declines across the collected subtractions, while the highest-m/z species can only be observed within the two early-eluting SCs subfractions (Fig. 2B). Despite the convoluted appearance of these mass spectra, the ionic masses can be readily determined using limited charge reduction[21,22]. For example, application of this technique to interpret the spectral feature localized within the m/z region 3500–4500 reveals its identity as 1:1 PF4/heparin complexes. These measurements are illustrated in Fig. 2B with a charge ladder produced by exposing the ionic population isolated at m/z 4383 to radical anions, which results in facile loss of up to four elementary charges. This charge ladder allows the mass of these ionic species to be calculated as 48.5 kDa, suggesting that the average mass of the heparin chain incorporated in these complexes is 16.8 kDa. Moving the precursor ion selection window to the m/z region 4500–6000 (the second distinct spectral feature in Fig. 2B) followed by limited charge reduction of the isolated ions also gives rise to a well-defined charge ladder. The mass range of the corresponding ionic species is 82–88 kDa, indicative of the presence of two PF4 tetramers within the complexes, and the mass of the

heparin component being 20–26 kDa (which corresponds to chains comprised of 66–86 saccharides assuming a sulfation density 2.7 per disaccharide, *vide supra*). Lastly, the masses of the ionic species giving rise to the third spectral feature are determined by selecting the precursor ions at m/z 6422. Limited charge reduction of these ions yields a 122–129 kDa mass range, indicative of the presence of three PF4 tetramers within the complex, and the mass of the heparin component falling within the 29–36 kDa range (96–120 saccharide unit-long chains, see Table S1 in Supplementary Material). Although these numbers appear high compared to the average size of UFH (15 kDa, or 50 monosaccharide units[29,30]), the size profiling of UFH using intact-mass MS supplemented with limited charge reduction reveals a broad distribution with the upper mass limit exceeding 40 kDa (Figure S2 in Supplementary Material).

The measured masses of SCs with various heparin/PF4 stoichiometries indicate that accommodation of a single PF4 tetramer by a heparin chain requires segments consisting of 30–40 monosaccharide units. Although this protein placement density is lower compared to that predicted by extrapolating the crystal structure of the PF4/fondaparinux complex[14], molecular modeling of PF4 interactions with long heparin chains (dp 40, dp70 and dp100) indicates that the polyanion possesses sufficient flexibility to wrap around the PF4 tetramers, thereby maximizing the electrostatic interactions (Fig. 3). The protein molecules in these structures are not only almost completely circumscribed with heparin chains, but also brought into proximity with each other such that the entire polyanion chain interacts with the positive charge basins on the proteins' surfaces.

Immune complexes formed by SC association with model HIT antibodies

The mass spectrum of PF4dp20 complexes incubated with a nearly-equimolar amount of the KKO antibodies displays an abundant ionic signal above m/z 6000 (Fig. 4) that can be deconvoluted to yield three components: the-lowest mass species (152.5 ± 1 kDa) corresponds to the antigen-free KKO molecules, while two others have masses consistent with $KKO \cdot PF4 \cdot (dp20)_2$ species (195.5 ± 1 kDa), and the antigen-saturated antibody, $KKO \cdot [PF4 \cdot (dp20)_2]_2$ and $[dp20 \cdot PF4] \cdot KKO \cdot [PF4 \cdot (dp20)_2]$ (237 ± 5 kDa), see Table S1 in Supplementary Material for more detail. No immune complexes contain more than a single antibody molecule, consistent with
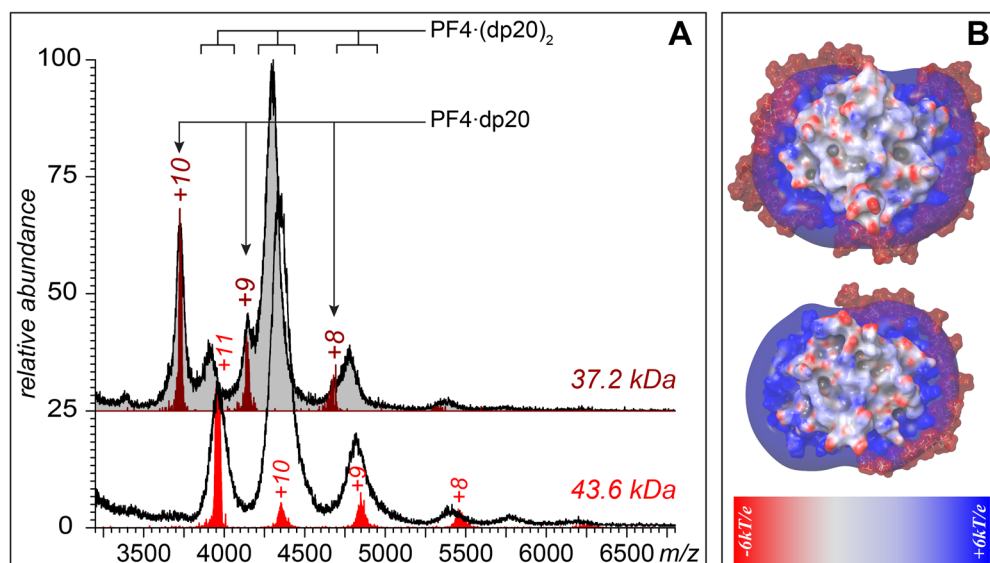

Fig. 1 | PF4 interaction with a fixed-length (twenty saccharide unit-long) heparin fragment. A Native MS of PF4/dp20 mixtures (*top*: 0.27 and 0.028 mg/mL, respectively; *bottom*: 0.27 and 0.045 mg/mL). The charge ladders shown in maroon and red were obtained by limited charge reduction of ionic populations at m/z 3,723 (top) and 3,953 (bottom). The two masses calculated based on these charge ladders

correspond to 1:1 (37.2 kDa) and 1:2 (43.6 kDa) protein:heparinoid stoichiometries. **B** Molecular modeling of PF4/dp20 interactions showing 1:1 and 1:2 protein/heparinoid complexes. The iso-potential surface ($6kT/e$) represents the positive belt around the protein, while the heparin chain is shown using a space-fill model (without the corresponding iso-potential surface).

the notion of a single neo-epitope generated on the PF4 surface following its association with heparin[14]. Au contraire, incubation of the highest-MW sub-fraction of SCs (having the highest PF4 load – up to three protein tetramers per single heparin chain, see Fig. 2) with a nearly-equimolar amount of KKO gives rise to abundant ionic signal extending well beyond m/z 10,000 (Fig. 5). While some spectral features can be readily recognized as the free antibody (m/z 6000–7500) and unconsumed SCs (m/z 4000–6000), assignment of the abundant ionic signal at m/z 7500–9000 cannot be made using native MS alone due to the lack of distinct features corresponding to individual charge states. Limited charge reduction allows the mass of the most abundant ions within this spectral region to be determined as 240 kDa (the red trace in Fig. 5). This value falls within the expected mass range for the 1:2:1 heparin/PF4/KKO complexes (Table S1 in Supplementary Material). Interestingly, the most abundant signal (populating the m/z region above 10,000) shows clearly discernable features representing individual charge states, which allows the ionic mass to be calculated as 424 ± 2.7 kDa. This value corresponds to 1:3:2 heparin/PF4/KKO complexes (Table S1 in Supplementary Material). No complexes of 1:3:3 heparin/PF4/KKO stoichiometry or above

were detected even when the antibody was present in molar excess (up to 33%).

Biological activity of the immune complexes built on SC templates

Small immune complexes prepared by incubation of KKO with a UFH/PF4 mixture were fractionated to produce components with different antibody content (Fig. 6). Consistent with the native MS data (*vide supra*), SEC chromatogram of the incubated mixture features two partially resolved peaks indicating the presence of either two or one KKO molecules in the immune complexes. The corresponding fractions (designated as A and B, respectively) were tested using serotonin release assay (SRA) with platelets collected from two donors. Even though borderline activity was detected for the crude sample prior to its fractionation (see the blue bars in Fig. 6), it is the fraction containing immune complexes with two antibody molecules per complex (fraction A) that showed the highest platelet-activating potential regardless of the nature of PF4 used to prepare the initial UFH/PF4 mixture (*i.e.*, both the recombinant PF4 and the platelet-derived PF4). While the
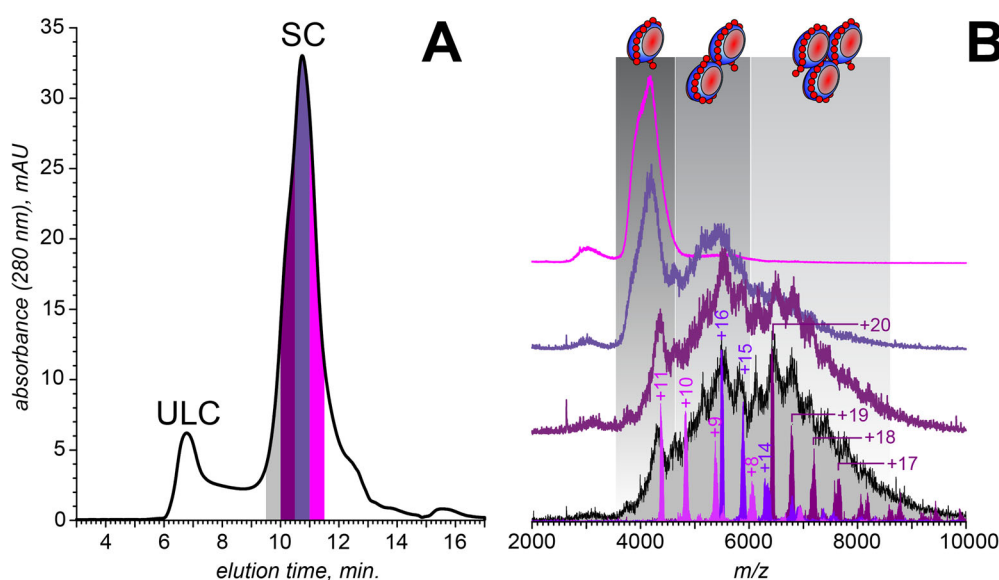

Fig. 2 | PF4 interaction with unfractionated heparin. A SEC of PF4 incubated with UFH (1.6 mg/mL and 0.67 mg/mL, respectively). **B** Native MS of the SC sub-fractions (as color-coded in **A**). The masses were determined using limited charge reduction, as illustrated for the highest-MW sub-fraction of SC.
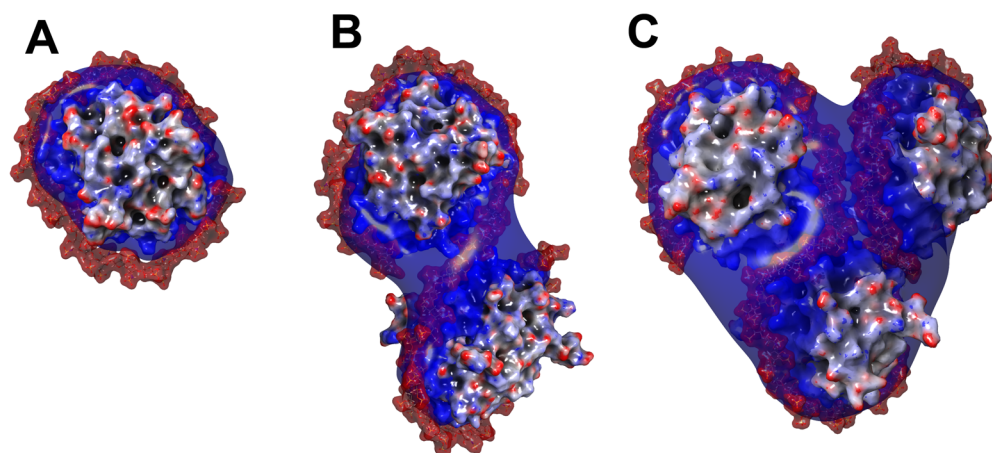

Fig. 3 | Molecular modeling of PF4-heparin interaction. Representative structures of dp40·PF4 (**A**), dp70·PF4 (**B**) and dp100·PF4 (**C**) complexes produced by molecular modeling (yielding 1:1, 1:2 and 1:3 heparin/PF4 complexes, respectively). The iso-potential surfaces (**A**: 5.5 kT/e and **B, C**: 7.5kT/e) represent the positive belts around the protein, while the heparin chain is shown using a space-fill model

(without a corresponding iso-potential surface). In all three cases the initial conformation of heparin was an extended chain; the complete wrapping of the heparin chain around the PF4 tetramers and formation of the compact structures took up to 200 ns of simulation time (see Figure S3 in Supplementary Material for details of the molecular modeling work and the convergence/reproducibility of simulations).
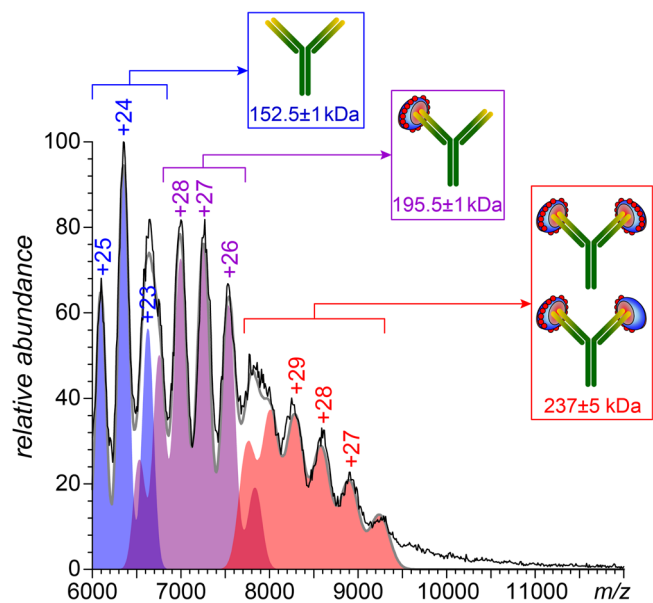
Fig. 4 | Native MS of PF4·dp20 complexes incubated with KKO (0.28 mg/mL and 0.06 mg/mL, respectively). The color-filled curves show contributions of three distinct species to the overall ionic signal (the sum of these contributions is shown with a gray trace).
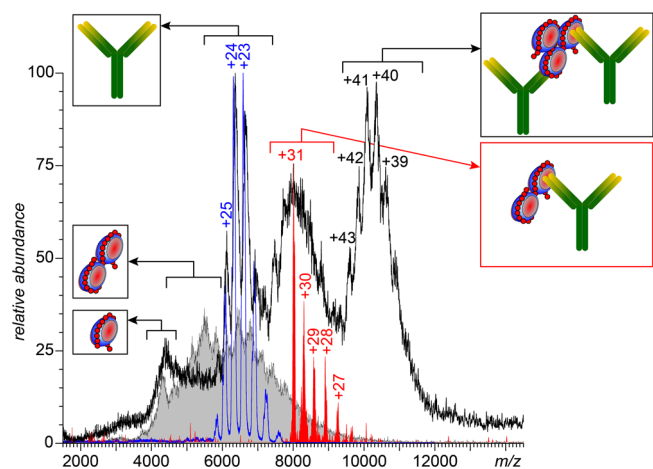

Fig. 5 | Native MS of an immune complex formed by KKO and the highest-MW sub-fraction of SCs. The blue and gray traces represent reference spectra of KKO and the highest-MW subfraction of SCs, respectively. The red trace represents the charge ladder produced by limited charge reduction of the ionic population selected at *m/z* 8,000.

SRA carried out with the platelets collected from another donor showed lower overall activity, the highest levels of serotonin release were once again registered for fraction A (see Figure S3 in Supplementary Material).

Discussion

Current understanding of the GAG/protein interactions invokes the notion of a multiplicity of mechanisms ranging from highly specific associations that are defined by surface complementarity (analogous to protein/protein binding) to non-specific binding that appears to lack any selectivity[31,32]. Electrostatic interactions are the most important forces driving protein association with polyanionic GAGs. The binding affinity is frequently determined by how well localization of the sulfate groups within the GAG chains matches the distribution of basic residues on the protein surface[31], a concept which is frequently referred to as a "sulfation code."[33,34] Heparin is the most densely charged GAG (on average, it carries three sulfate groups
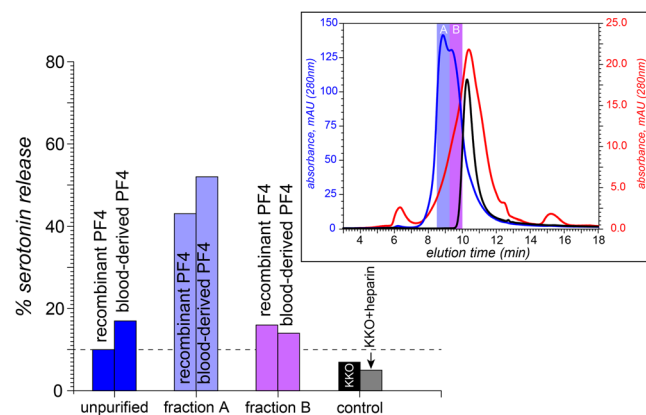

Fig. 6 | In vitro platelet activation by the immune complexes assembled on SCs. SRA data showing the platelet activation by KKO incubated with a UFH/PF4 mixture without fractionation of the immune complexes (blue bars), and after isolating fractions containing two and one KKO molecules per immune complex (fractions A and B represented with the violet and purple bars, respectively); platelet activation is shown as the percent release of ^{14}C-serotonin. The left and right bars in each group represent the data acquired with recombinant and platelet-derived forms of PF4, respectively. The control measurements are shown with the black and gray bars (KKO alone and KKO/heparin mixture, respectively). The chromatogram in the inset (blue trace) shows the elution windows during which the two fractions (A and B) were collected; the reference chromatograms of the free KKO (black) and the starting UFH/PF4 mixture (red) are shown.

per disaccharide unit in addition to a single carboxylate). The high charge density and its relatively even distribution across the heparin chain (unlike heparan sulfate, where short highly sulfated segments are spaced by relatively long low charge-density regions[9,35]) provides for an ideal match to the positive charge distribution across the PF4 surface (which forms an equatorial belt around the protein tetramer[16,36], giving rise to nearly symmetric toroidally-shaped isopotential surfaces). This naturally invites a suggestion that a sufficiently long heparin chain should envelope the protein molecule to maximize the enthalpic gains due to favorable electrostatic interactions[16]. Even though heparin maintains extended/stretched conformations in solution[37,38], its chain flexibility is sufficient to allow the PF4 tetramer to be neatly circumscribed along its positive charge belt (indeed, heparin's Kuhn segment length of 9 ± 2 nm[27] is notably lower compared to the PF4 tetramer diameter of 52 ± 3 nm).

The favorable flexibility parameters of the heparin chains and their high charge density suggest that the "wrap-around" mode of PF4/heparin interactions is favored thermodynamically, which is also confirmed by the results of MD simulations (Fig. 3). Although the sheer size of the UFH/PF4 complexes makes the exhaustive atomic-level exploration of the entire conformational space available to such molecular entities unfeasible at present (explicit modeling remains problematic for GAG chains above decamers[32,39,40]), the MD simulations carried out in this study certainly demonstrate that the "wrap-around" mode of association is feasible. At the same time, one must also consider a possibility of kinetic effects preventing formation of structures that maximize the electrostatics-driven enthalpic gains. For example, initial random polyanion-protein contacts may give rise to metastable structures in which the electrostatic interactions are not maximized, but the kinetic barriers separating them from the lower-energy minima are sufficiently high to guarantee their survival for long time periods. While such a scenario (a "Velcro effect") appears feasible, the experimentally observed correlation between the heparin chain length and the number of PF4 tetramers it can accommodate (Fig. 2B and Table S1 in Supplementary Material) provides a strong argument against it. Native MS clearly indicates that each PF4 tetramer in heparin·(PF4)$_n$ complexes recruits a segment consisting of 35–40 saccharide units, which is indeed the length required to circumscribe the entire protein along its positive charge belt (Fig. 3). The thermodynamically favored polyanion collapse onto the

polycationic surface of PF4 also explains the failure of the relatively short heparinoids to bridge two PF4 tetramers (unlike proteins with less extensive basins of the positive charge - such as neutrophil elastase or fibroblast growth factor - which can form dimers bridged by heparinoids as short as decasaccharides[25,41]). Our previous work[23] demonstrated that such heparinoids (dp10) are incapable of PF4 bridging[23], and the results of the present study indicate that even heparin fragments that are twice as long (dp20) are not sufficiently large to enable PF4 bridging.

While the average length of UFH chains is *ca.* 50 saccharides, MS analysis assisted by limited charge reduction reveals a broad size distribution with the largest (but less abundant) heparin molecules exceeding 40 kDa (corresponding to chains that are over 120 monosaccharide unit-long, see Figure S2 in Supplementary Material). This length is sufficient to allow complete wrapping of three PF4 tetramers by a single heparin chain, yielding heparin·(PF4)$_3$ assemblies (the largest ones detected by native MS measurements, Fig. 3). The absence of the heparin/PF4 assemblies with higher protein load among SCs is fully consistent with the "wrap-around" model of the protein-polyanion interaction (higher binding stoichiometry would require polyanionic chains that are sufficiently longer than those present in UFH).

The tight wrapping of the protein molecules by heparin chains within the SCs revealed by native MS measurements and molecular modeling work provides an explanation for another intriguing observation, namely the mismatch between the number of PF4 tetramers and antibodies (KKO) within the largest immune complexes built upon SCs. Indeed, the tight packing of the protein molecules within SCs results in steric hindrance that prevents association of more than a single antibody with PF4 on either side of the complex (Fig. 7 and Figure S5 in Supplementary Material). In this case, KKO binding to the (PF4)$_3$·heparin complex is possible only in the trans conformation, thereby limiting the antibody load of such complexes to two, exactly as observed by native MS (Fig. 5). Despite their modest antibody load, such complexes are capable of activating platelets as shown by the results of in vitro testing (Fig. 6). This raises an intriguing question: is the close approximation of only two FcγRIIa receptors via binding to a single KKO$_2$·(PF4)$_3$·heparin complex sufficient for triggering platelet activation, or is the receptor pairing only a first step in assembling large FcγRIIa clusters, driven by polymerization of the platelet-bound KKO$_2$·(PF4)$_3$·heparin complexes on the cell surface (Fig. 8)? The ability of KKO to promote oligomerization of PF4/heparin complexes has been previously proposed[42], and even though the KKO-mediated polymerization of SCs in solution was not observed in our work, it is possible that it is accelerated on the platelet surface due to the dimensionality reduction (from 3D in solution to 2D on the platelet surface). Should this "on-the-membrane" polymerization of small immune complexes occur, it would culminate in the platelet activation triggered by FcγRIIa clustering and the ensuing phosphorylation cascade[5,43]. The resulting platelet degranulation and release of PF4 will create a positive feed-back loop in HIT progression[44,45]. Furthermore, there is a growing realization that in addition to platelets, pathogenesis of HIT-related thrombosis involves other blood cells[46], most of which constitutively express FcγRIIa[47] and, therefore, can be activated by the heparin/PF4-templated immune complexes. Neutrophils are particularly important players in this respect due to their ability to release neutrophil extracellular traps (NETs)[48] upon activation, which – due to the high content of long polyanions, such as DNA and polyphosphates – can act synergistically with heparin to provide additional scaffolds for assembling large PF4/polyanion complexes.

Our study has been focused primarily on the small PF4/heparin complexes, while the ULCs remained beyond its scope. However, the SC architecture revealed in this work provides important clues vis-à-vis the ULC structure and its assembly process. Since even the longest heparin chains cannot accommodate more than three PF4 tetramers, formation of the large complexes (exceeding 0.65 MDa by early estimates[8] and averaging *ca.* 3 MDa according to our own estimates—see Figure S6 in Supplementary Material) must proceed through the association of multiple heparin chains and PF4 tetramers. Since heparin chains maximize the electrostatic interactions with PF4 by circumscribing it, the heparin/PF4 complex

polymerization process would proceed beyond the 1:3 stoichiometry (the observed SC limit) only if at every stage of the process there is a mismatch between the length of the unaccommodated heparin segment and the circumference of the PF4 tetramer being added to this nascent complex (see Figure S7 in Supplementary Material). Once these two dimensions become comparable, the growth of the complex stops, since neither GAG nor protein components of the complex will have any vacant high-charge density segments left to support further growth. This model is consistent with the notion of the ULC composition conforming to 1:1 stoichiometry, and our rough estimations of the ULC mass based on the model that correlates ionic *m/z* value and charge (*z*) in native MS[49] yield *ca.* 3 MDa (Supplementary Material), suggesting that the number of PF4 tetramers in a single ULC particle exceeds 50. Even if a significant proportion of these molecules is inaccessible to anti-PF4 antibodies due to the steric hindrance, these particles should be able to accommodate a large number of antibodies and potentially lead to the formation of large FcγRIIa clusters on the platelet surface. Nevertheless, the ability of the SC-based immune complexes to activate platelets (Fig. 8) should not be overlooked. This mechanism does not appear to be unique to HIT, but is likely involved in other pathologies precipitated by platelet activation with antibody cross-linking.

The combination of native MS with molecular modeling allows molecular architecture to be established for the PF4/heparin small complexes and the corresponding immune complexes. Heparin chains possess sufficient flexibility to wrap around polycationic PF4 molecules to maximize electrostatic attraction. This mode of interaction dictates the maximum size of SCs (up to three protein molecules bound to a single heparin chain), as accommodation of a single PF4 tetramer within the complex requires a polyanionic segment consisting of 30–40 saccharide units. Despite the presence of up to three PF4 molecules within SCs, no more than two anti-PF4 antibodies associate with a single SC. Surprisingly, even this relatively low level of antibody loading is sufficient to trigger platelet activation. It remains to be seen whether bringing only two FcγRIIa receptors on the
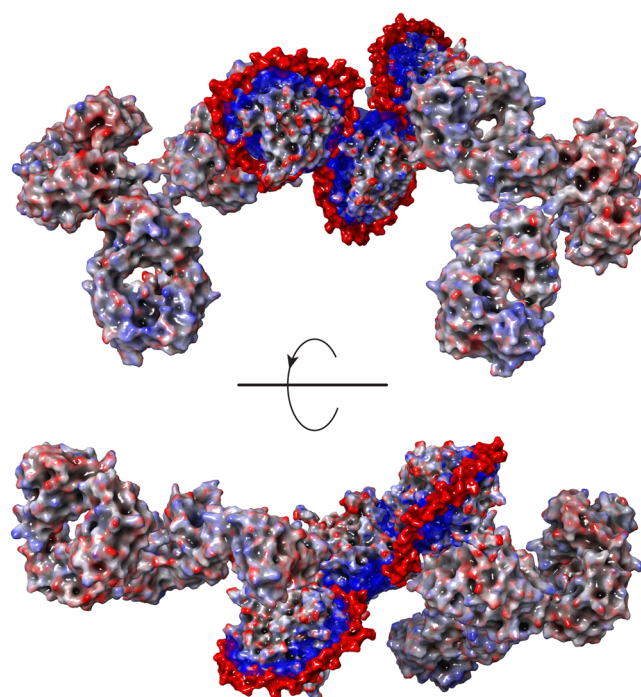

Fig. 7 | Molecular modeling of immune complexes assembled on SCs. A representative conformation of the dp100·(PF4)$_3$·KKO$_2$ complex obtained by docking two KKO Fab segments to the dp100·(PF4)$_3$ complex followed by a 500 ns MD simulation and energy minimization. Both Fab segments in the energy-minimized structure were extended to the full-length IgG molecules followed by another cycle of energy minimization.
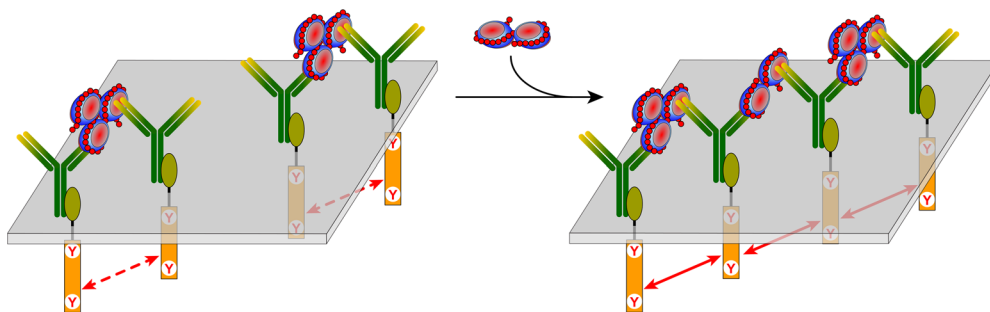
Fig. 8 | A schematic representation of two scenarios of platelet activation by immune complexes built upon SC/KKO association. *Left*: KKO$_2$·(PF4)$_3$·heparin, the largest SC/KKO complexes produced in solution, bind to the FcγRIIa receptors on the platelet surface, which leads to the pairing of the ITAM segments and enables their activation. *Right*: the receptor-bound KKO$_2$·(PF4)$_3$·heparin complexes are cross-linked by SCs via the "vacant" Fab arms of the antibody molecules, giving rise to large FcγRIIa clusters on the platelet surface and close localization of multiple ITAM segments.

platelet surface into a close proximity with each other and the ensuing cross-phosphorylation of their ITAM elements activates the platelet by setting in motion the Syk pathway[50] or further assembly of large receptor clusters on the cell surface is precipitated by polymerization of small immune complexes driven by the dimensionality reduction. Although the highly pathogenic ULCs largely remain beyond the scope of native MS at present, the structural properties of SCs revealed in this study provide important clues as to how these large, MDa-sized PF4/heparin assemblies are produced. The continuous improvements in native MS technology and expansion of its scope leave no doubt that the emerging model of ULC architecture will be tested in the near future, allowing the mechanisms of HIT and related thrombotic disorders to be thoroughly studied at the molecular level.

Methods

Materials

Both UFH and dp20 were purchased from Galen Laboratory Supplies (North Haven, CT). The recombinant form of human PF4 was expressed and purified using a protocol described elsewhere[51], and blood-derived human PF4 was obtained from Hematologic Technologies (now Prolytix, Essex Junction, VT). The KKO mAb was obtained using KKO hybridoma clone 31.2.57.A7 cell line (ATCC Manassas, VA). These cells were first thawed in HCELL-100 hybridoma serum free media (Wisent Bioproducts, Saint Jean-Baptiste, QC, Canada) supplemented with 200 mM L-glutamine (Thermo Fisher Scientific, Waltham, MA) and 10 000 U/mL penicillin + 10 000 µg/mL streptomycin (Thermo Fisher Scientific) then transferred to T-25 vented tissue culture flasks (Sarstedt, Nümbrecht,Germany) and incubated at 37 °C and 5% CO$_2$ for 3 days. KKO cells were then diluted 1/10 and passaged every 3–5 days. Passages 3, 4 and 5 were overgrown for an additional 10–14 days after which the supernatant was collected and frozen at −80 °C. KKO was then purified using Protein A Sepharose beads (Thermo Fisher Scientific) packed in an Econo-chromatography column (BioRad, Hercules, CA) and washed 3 times with phosphate buffered saline (PBS). Thawed KKO supernatant was then run through the Protein A column and after the beads were washed with PBS, KKO antibody was eluted with 0.1 M Glycine pH 2.8 in 1 mL aliquots and immediately neutralized with 100 µL of 1.5 M Tris pH 8.8. Next, the optical density (OD) at 280 nm was measured using a spectrophotometer (Eppendorf, Hamburg, Germany) and individual fractions with KKO were assessed for purity using SDS-PAGE and pooled. Finally, the concentration of the pooled fractions was measured and KKO binding to biotinylated PF4 was assessed using an in-house enzyme immunoassay. The quality of all biological products used in this study was verified using MS or LC/MS analysis. PF4/heparin and PF4/dp20 complexes were prepared by incubation of the protein/GAG mixtures in 150 mM ammonium acetate at 37 °C for 30 min using mixing stoichiometries as described in the text. SEC fractionation of SCs carried out using a Sepax Nanofilm SEC-500 (Sepax, Newark, DE) on an HP1200 (Agilent Technologies, Santa Clara, CA) chromatograph. All protein and heparin solutions for MS analyses were prepared in 150 mM ammonium acetate, pH adjusted to 6.9.

Mass spectrometry

All native MS measurements were carried out using Synaprt G2 and Synapt G2Si (Waters Corp., Milford, MA) hybrid quadrupole/time-of-flight mass spectrometers equipped with nanospray ionization sources. The following set of parameters was used in the ESI interface region to ensure the survival of non-covalent complexes: capillary voltage, 1.4 kV; sampling cone voltage, 80 V; source offset, 80 V; trap CE, 4 V; trap DC bias, 3 V; and transfer CE, 0 V. Isolation of ionic populations in the trap cell for subsequent limited charge reduction measurements was performed by setting the quadrupole LM resolution values in the range of 4.0–4.5. Charge reduction of the selected polycationic ions was triggered by introducing 1,3-dicyanobenzene anions after setting the trap wave height to 0.2 V and optimizing the discharge current.

In vitro platelet activation studies

Two sets of PF4/heparin complexes were prepared and tested for their ability to activate platelets using the serotonin release assay (SRA)[52], one containing the recombinant form of human PF4, and the other containing platelet-derived PF4. In each case PF4 was incubated with UFH (final concentrations 0.126 and 0.285 mg/mL, respectively) at 37 °C for 30 min in 1X PBS buffer, followed by addition of KKO (final concentration 3.4 mg/mL). The resulting immune complexes were fractionated on SEC, and the two most abundant fractions were tested twice using platelets from two different donors. The control tests were carried out using 1.95–2.24 mg/mL KKO without PF4/heparin complexes in the media.

Molecular modeling

All modeling studies in this work were performed with the Maestro platform (Schrödinger Release 2022-3, Schrödinger LLC, New York, NY) using OPLS4 force field, which has improved accuracy for sulfur-containing moieties[53]. The initial structure of PF4 and KKO Fab were taken from the crystal structure (PDB: 4R9Y). The Schrödinger Protein Preparation Wizard tool was used to optimize the proteins by removing water molecules and adding the missing hydrogen atoms, side chains, and bond orders. The missing residues in the N-terminal segment of PF4 (residues 1–6, missing in the crystal structure) were appended to PF4 followed by energy minimization (until the maximum change in distance between atoms drops below 0.1 Å). The fully sulfated heparin chains were generated by modifying the solution structure of dp24 (PDB: 3IRJ) to incorporate the appropriate modifications. Subsequently, the chains were either shortened or extended to achieve the desired length. The conformation of the PF4/heparin complexes used in MD simulations and more details for MD simulation can be found in Supplementary Material. All SPC water systems were built by system builder as a Desmond

application in Schrödinger Suite. In all cases, the periodic boxes employed in this study were orthorhombic in shape, with a buffer region of 10 Å maintained in all three dimensions between the solute and the boundaries of the box. This buffer helps to minimize interactions between the solute and its periodic images, ensuring accurate simulations and reducing boundary effects. The proper amount of Na^+ ion and Cl^- ion were added to neutralize the system and reach the salt concentration corresponding to the physiological ionic strength (150 mM). The solvated PF4/heparin systems were first equilibrated using two rounds of NVT simulations, which would be slowly heated up from 10 K to 310 K in a total of 100 ps and 12 ps, respectively, during which all protein heavy atoms were restrained using harmonic potentials. Another two rounds of 12-ps NPT simulations, where protein heavy atoms were similarly restrained, were executed at 1 atm, 10 K and 310 K, respectively. The next NPT simulation was then carried out at 310 K and 1 atm for a total of 24 ps with no restraints on protein heavy atoms for pre-equilibration. The production simulations were run under NPT conditions at 310 K and 1 atm for various time lengths. Recording interval is set as 100 ps. Noose-Hoover thermostat was used to control the temperature and barostat with volume move attempt every 2 ps to control the pressure. Lengths of all bonds involving hydrogen atoms were constrained using the SHAKE algorithm to allow for an integration time step of 2 fs with RESPA algorithm. Long-range electrostatic interactions were treated using the particle mesh Ewald method, and the short-range van der Waals interactions were treated with the cutoff at 9 Å. No enhanced sampling methods are needed as the complexes formations are convergent at the brute-force MD simulation timescale.

In the study of PF4/dp100 complexes, three replicates were performed with different initial states to assess the stability of the resulting complexes (Figure S3 in Supplementary Material). The first replicate was performed starting with putting two PF4 tetramers close to the two ends of dp100 with a distance of 30 Å to make sure that the proteins would bind to dp100. After 100 ns simulation, the PF4 tetramers were wrapped by dp100 at the two ends, whose structure was used as the initial structure of dp100·(PF4)$_3$ complex by putting the third PF4 tetramer to roughly middle of dp100 with a distance of 50 Å. In the second replicate, all 3 PF4 tetramers were randomly positioned near dp100 with a distance of about 50 Å. For the third replicate, one PF4 tetramer was positioned close to the middle of dp100, but with a distance greater than 50 Å. After 100 ns simulation, the other 2 PF4 tetramers were added to the complex with a distance exceeding 50 Å. Regarding the PF4/dp70 complexes, all initial structures ensured that the PF4 tetramers were positioned at distances greater than 50 Å from the heparin chains. This arrangement allowed examination of the behavior of the proteins in the absence of direct binding.

Statistics and reproducibility

All MS measurements have been carried out in triplicates to ensure reproducibility of the measurements. Molecular modeling studies of all relevant systems have been carried out in triplicates as well to demonstrate the convergence of the resulting structures (formation of compact PF4/heparin assemblies); see Figure S3 in the Supplementary Material as an example of the convergence study. The biological effects (the platelet activation ability) of the small immune complexes were evaluated in SRA measurements (*vide supra*) using platelets from two independent donors (refer also to Figure S4 in the Supplementary Material).

Reporting summary

Further information on research design is available in the Nature Portfolio Reporting Summary linked to this article.

Data availability

The data presented in the manuscript have been made publicly available at no charge (https://doi.org/10.6084/m9.figshare.25148774.v3)[54].

References

1. Karshovska, E., Weber, C. & von Hundelshausen, P. Platelet chemokines in health and disease. *Thromb. Haemost.* **110**, 894–902 (2013).
2. Kasper, B. & Petersen, F. Molecular pathways of platelet factor 4/CXCL4 signaling. *Eur. J. Cell Biol.* **90**, 521–526 (2011).
3. Weismann, R. E. & Tobin, R. W. Arterial embolism occurring during systemic heparin therapy. *AMA Arch. Surg.* **76**, 219–225 (1958).
4. Ivanov, D. G. et al. Reverse engineering of a pathogenic antibody reveals the molecular mechanism of vaccine-induced immune thrombotic thrombocytopenia. *J. Am. Chem. Soc.* **145**, 25203–25213 (2023).
5. Qiao, J. L., Al-Tamimi, M., Baker, R. I., Andrews, R. K. & Gardiner, E. E. The platelet Fc receptor, Fc gamma RIIa. *Immunol. Rev.* **268**, 241–252 (2015).
6. Jevtic, S. D. & Nazy, I. The COVID complex: a review of platelet activation and immune complexes in COVID-19. *Front. Immunol.* **13**, 807934 (2022).
7. Suvarna, S. et al. Determinants of PF4/heparin immunogenicity. *Blood* **110**, 4253–4260 (2007).
8. Rauova, L. et al. Ultralarge complexes of PF4 and heparin are central to the pathogenesis of heparin-induced thrombocytopenia. *Blood* **105**, 131–138 (2005).
9. Casu, B. & Lindahl, U. Structure and biological interactions of heparin and heparan sulfate. *Adv. Carbohydr. Chem. Biochem.* **57**, 159–206 (2001).
10. Rabenstein, D. L. Heparin and heparan sulfate: structure and function. *Nat. Prod. Rep.* **19**, 312–331 (2002).
11. Kim, J. Y. et al. Quantitative pattern analysis of the N-terminally processed isoforms of platelet factor-4 in serum. *Rapid Commun. Mass Spectrom.* **27**, 521–530 (2013).
12. Delcea, M. & Greinacher, A. Biophysical tools to assess the interaction of PF4 with polyanions. *Thromb. Haemost.* **116**, 783–791 (2016).
13. Greinacher, A. et al. Close approximation of two platelet factor 4 tetramers by charge neutralization forms the antigens recognized by HIT antibodies. *Arterioscler. Thromb. Vasc. Biol.* **26**, 2386–2393 (2006).
14. Cai, Z. et al. Atomic description of the immune complex involved in heparin-induced thrombocytopenia. *Nat. Commun.* **6**, 8277 (2015).
15. Arepally, G. M. et al. Characterization of a murine monoclonal antibody that mimics heparin-induced thrombocytopenia antibodies. *Blood* **95**, 1533–1540 (2000).
16. Stuckey, J. A., St Charles, R. & Edwards, B. F. A model of the platelet factor 4 complex with heparin. *Proteins* **14**, 277–287 (1992).
17. Abzalimov, R. R., Dubin, P. L. & Kaltashov, I. A. Glycosaminoglycans as naturally occurring combinatorial libraries: developing a mass spectrometry-based strategy for characterization of anti-thrombin interaction with low molecular weight heparin and heparin oligomers. *Anal. Chem.* **79**, 6055–6063 (2007).
18. Nugent, M. A., Zaia, J. & Spencer, J. L. Heparan sulfate-protein binding specificity. *Biochem. (Mosc.)* **78**, 726–735 (2013).
19. Crown, S. E., Yu, Y., Sweeney, M. D., Leary, J. A. & Handel, T. M. Heterodimerization of CCR2 chemokines and regulation by glycosaminoglycan binding. *J. Biol. Chem.* **281**, 25438–25446 (2006).
20. Foreman, D. J. & McLuckey, S. A. Recent developments in gas-phase ion/ion reactions for analytical mass spectrometry. *Anal. Chem.* **92**, 252–266 (2020).
21. Abzalimov, R. R. & Kaltashov, I. A. Electrospray ionization mass spectrometry of highly heterogeneous protein systems: protein ion charge state assignment via incomplete charge reduction. *Anal. Chem.* **82**, 7523–7526 (2010).

22. Kaltashov, I. A., Ivanov, D. G. & Yang, Y. Mass spectrometry-based methods to characterize highly heterogeneous biopharmaceuticals, vaccines, and nonbiological complex drugs at the intact-mass level. *Mass Spectrom. Rev.* **43**, 139–165 (2024).

23. Niu, C., Yang, Y., Huynh, A., Nazy, I. & Kaltashov, I. A. Platelet factor 4 interactions with short heparin oligomers: implications for folding and assembly. *Biophys. J.* **119**, 1371–1379 (2020).

24. Bisio, A. et al. Determination of the molecular weight of low-molecular-weight heparins by using high-pressure size exclusion chromatography on line with a triple detector array and conventional methods. *Molecules* **20**, 5085–5098 (2015).

25. Minsky, B. B., Dubin, P. L. & Kaltashov, I. A. Electrostatic forces as dominant interactions between proteins and polyanions: an ESI MS study of fibroblast growth factor binding to heparin oligomers. *J. Am. Soc. Mass Spectrom.* **28**, 758–767 (2017).

26. Shi, D. et al. New insights into the binding of PF4 to long heparin oligosaccharides in ultralarge complexes using mass spectrometry. *J. Thromb. Haemost.* **21**, 3608–3618 (2023).

27. Pavlov, G., Finet, S., Tatarenko, K., Korneeva, E. & Ebel, C. Conformation of heparin studied with macromolecular hydrodynamic methods and X-ray scattering. *Eur. Biophys. J.* **32**, 437–449 (2003).

28. Niu, C., Zhao, Y., Bobst, C. E., Savinov, S. N. & Kaltashov, I. A. Identification of Protein Recognition Elements within Heparin Chains Using Enzymatic Foot-Printing in Solution and Online SEC/MS. *Anal. Chem.* **92**, 7565–7573 (2020).

29. Capila, I. & Linhardt, R. J. Heparin-protein interactions. *Angew. Chem. Int. Ed. Engl.* **41**, 391–412 (2002).

30. Gong, F. et al. Processing of macromolecular heparin by heparanase. *J. Biol. Chem.* **278**, 35152–35158 (2003).

31. Kjellen, L. & Lindahl, U. Specificity of glycosaminoglycan-protein interactions. *Curr. Opin. Struct. Biol.* **50**, 101–108 (2018).

32. Nagarajan, B., Holmes, S. G., Sankaranarayanan, N. V. & Desai, U. R. Molecular dynamics simulations to understand glycosaminoglycan interactions in the free- and protein-bound states. *Curr. Opin. Struct. Biol.* **74**, 102356 (2022).

33. Gama, C. I. et al. Sulfation patterns of glycosaminoglycans encode molecular recognition and activity. *Nat. Chem. Biol.* **2**, 467–473 (2006).

34. Habuchi, H., Habuchi, O. & Kimata, K. Sulfation pattern in glycosaminoglycan: does it have a code? *Glycoconj. J.* **21**, 47–52 (2004).

35. Shi, X. & Zaia, J. Organ-specific heparan sulfate structural phenotypes. *J. Biol. Chem.* **284**, 11806–11814 (2009).

36. Zhang, X., Chen, L., Bancroft, D. P., Lai, C. K. & Maione, T. E. Crystal structure of recombinant human platelet factor 4. *Biochemistry* **33**, 8361–8366 (1994).

37. Rubinson, K. A., Chen, Y., Cress, B. F., Zhang, F. & Linhardt, R. J. Heparin's solution structure determined by small-angle neutron scattering. *Biopolymers* **105**, 905–913 (2016).

38. Khan, S., Gor, J., Mulloy, B. & Perkins, S. J. Semi-rigid solution structures of heparin by constrained X-ray scattering modelling: new insight into heparin-protein complexes. *J. Mol. Biol.* **395**, 504–521 (2010).

39. Marcisz, M., Maszota-Zieleniak, M., Huard, B. & Samsonov, S. A. Advanced molecular dynamics approaches to model a tertiary complex APRIL/TACI with long glycosaminoglycans. *Biomolecules* **11**, 1349 (2021).

40. Marcisz, M., Zacharias, M. & Samsonov, S. A. Modeling protein-glycosaminoglycan complexes: does the size matter? *J. Chem. Inf. Model.* **61**, 4475–4485 (2021).

41. Niu, C., Du, Y. & Kaltashov, I. A. Towards better understanding of the heparin role in NETosis: Feasibility of using native mass spectrometry to monitor interactions of neutrophil elastase with heparin oligomers. *Int. J. Mass Spectrom.* **463**, 116550 (2021).

42. Sachais, B. S. et al. Dynamic antibody-binding properties in the pathogenesis of HIT. *Blood* **120**, 1137–1142 (2012).

43. Yeung, J., Li, W. & Holinstat, M. Platelet signaling and disease: targeted therapy for thrombosis and other related diseases. *Pharmacol. Rev.* **70**, 526–548 (2018).

44. Arepally, G. M. & Cines, D. B. Pathogenesis of heparin-induced thrombocytopenia. *Transl. Res.* **225**, 131–140 (2020).

45. Warkentin, T. E. Platelet-activating anti-PF4 disorders: an overview. *Semin. Hematol.* **59**, 59–71 (2022).

46. Arepally, G. M. & Padmanabhan, A. Heparin-Induced Thrombocytopenia: A Focus on Thrombosis. *Arterioscler. Thromb. Vasc. Biol.* **41**, 141–152 (2021).

47. van Rees, D. J., Szilagyi, K., Kuijpers, T. W., Matlung, H. L. & van den Berg, T. K. Immunoreceptors on neutrophils. *Semin. Immunol.* **28**, 94–108 (2016).

48. Perdomo, J. et al. Neutrophil activation and NETosis are the major drivers of thrombosis in heparin-induced thrombocytopenia. *Nat. Commun.* **10**, 1322 (2019).

49. Yang, Y., Ivanov, D. G. & Kaltashov, I. A. The challenge of structural heterogeneity in the native mass spectrometry studies of the SARS-CoV-2 spike protein interactions with its host cell-surface receptor. *Anal. Bioanal. Chem.* **413**, 7205–7214 (2021).

50. Mócsai, A., Ruland, J. & Tybulewicz, V. L. The SYK tyrosine kinase: a crucial player in diverse biological functions. *Nat. Rev. Immunol.* **10**, 387–402 (2010).

51. Huynh, A. et al. Development of a high-yield expression and purification system for platelet factor 4. *Platelets* **29**, 249–256 (2018).

52. Sheridan, D., Carter, C. & Kelton, J. G. A diagnostic test for heparin-induced thrombocytopenia. *Blood* **67**, 27–30 (1986).

53. Lu, C. et al. OPLS4: improving force field accuracy on challenging regimes of chemical space. *J. Chem. Theory Comput.* **17**, 4291–4300 (2021).

54. Kaltashov, I. (Raw data files for the manuscript "Molecular architecture and platelet-activating properties of small immune complexes assembled on intact heparin and their possible involvement in heparin-induced thrombocytopenia" by Yang et al. Figshare. Dataset. https://doi.org/10.6084/m9.figshare.25148774.v3, (2024).

Author contributions

Y.Y. prepared the samples, carried out MS measurements and interpreted the data; Y.D. prepared the samples for biological testing and carried out molecular modeling work; D.I. carried out MS measurements and interpreted the data; C.N. carried out MS measurements; R.C. expressed the recombinant forms of PF4 and KKO; J.S. carried out the platelet activation measurements and interpreted the data; I.N. designed the biological testing of the small immune complexes and provided oversight for the recombinant protein production; I.K. designed the study, provided oversight of the experimental work (MS measurements), interpreted the data and drafted the manuscript. All co-authors have participated in editing the manuscript and gave their consent to its final (submitted) version.

Competing interests

The authors declare no competing interests.

Additional information

Supplementary information The online version contains supplementary material available at https://doi.org/10.1038/s42003-024-05982-4.

Correspondence and requests for materials should be addressed to Igor A. Kaltashov.

Peer review information *Communications Biology* thanks Rajarshi Roy and Di Wu for their contribution to the peer review of this work. Primary Handling Editors: Gene Chong and Christina Karlsson Rosenthal.

Reprints and permissions information is available at http://www.nature.com/reprints

Publisher's note Springer Nature remains neutral with regard to jurisdictional claims in published maps and institutional affiliations.